Novel Ni/MgO Catalysts from mesoporous $MgCO_3$ for Highly Efficient CO methanation: Effects of Al and Si Stabilization

Wenming Hao,[a] Maria Vall,[b] Yufei Shi,[a] Qianqian Wang,[a] Maria Strømme,[b] Xiaoliang Yan,*[a] Ocean Cheung,*[b] Ruifeng Li[a]

[a]College of Chemistry and Chemical Engineering, Taiyuan University of Technology, Taiyuan, Shanxi 030024, China.

[b]Division for Nanotechnology and Functional Materials, Department of Materials Science and Engineering, Uppsala University, Uppsala, SE-751 21, Sweden.

Abstract

Methanation of syngas is a possible way to produce synthetic natural gas. Ni has been proven to be a good and cost-effective catalyst for this reaction. Here we have synthesized Ni/MgO catalyst using mesoporous magnesium carbonate (MMC) as a precursor. Addition of Al_2O_3 and SiO_2 to MMC were made and the different MMC based materials were then impregnated with $Ni(NO_3)_2$ and calcined to generate the catalysts. Addition of Al_2O_3 showed an improvement in the catalytic performance compared to the NiO/MgO catalyst. The catalyst containing Al_2O_3 had a CO conversion close to 100 % at 350 °C and a high selectivity and yield for CH_4. The better performance of the aluminum containing catalyst was believed to be an effect of a better dispersion of Ni at the surface of the catalyst.

1. Introduction

Natural gas is a common source of energy, but with increasing demand and a shortage of resources, the possibility of producing synthetic natural gas (SNG) is becoming increasingly attractive. Natural gas has a high energy density. It is also cleaner than other fossil fuels and there is already an existing infrastructure i.e. gas pipes for transportation[1]. These advantages makes the production of SNG highly desirable. Methanation is the process of converting carbon oxides (CO or CO_2) into natural gas (CH_4). The process was first reported in 1902 by Sabatier and Senderens using nickel as a catalyst to promote the reaction[2]. Methanation of carbon oxide

have mostly been used in industry as a method of removing CO from H_2 streams in ammonia plants [3]. More recently the possibility of using methanation of syngas to produce SNG for energy have been given more attention.

The methanation reaction is thermodynamically favorable, but a catalyst is usually needed to obtain a good conversion rate. Nickel is to this day the most used catalyst for this reaction because of its high methanation activity, good availability and low cost[4].

One of the drawbacks with using nickel as a catalyst is that it suffers from sintering and carbon deposition at higher temperatures. Sintering causes the deactivation and subsequent reduction of catalytic activity [4]. Furthermore, Ni-based catalysts has low activity and selectivity[5] at low temperatures (i.e. under 400°C) . Supporting Ni-catalyst is a way to stabilize the catalyst by reducing sintering as well as the carbon deposition[6]. For the supported Ni catalyst, the performance at low temperatures have shown to be affected by the interaction between the Ni and the support[5]. Different types of materials as well as mixtures of different materials have been tested as Ni supports, (e.g. Al_2O_3[7] MgO[8], CeO_2[4], MOFs[5], SiO_2[9]) to stabilize and facilitate a high catalytic conversion, selectivity and possibly lowering the operating temperature.

Mesoporous magnesium carbonate (MMC) is synthesized by pressurizing a mixture of MgO and MeOH with CO_2. The synthesis results in a colloidal suspension of nanoparticles. These nanoparticles form a highly porous amorphous solid with a surface area of up to over 700 m^2/g[10, 11]upon drying into a powder form. In this paper MMC doped with Al_2O_3 and SiO_2 nanoparticles where impregnated with $NiNO_3$. The catalytic performance of the resulting materials was evaluated.

2. Materials and methods

2.1. Preparation of MMC (-Al, -Si)

The synthesis of MMC have previously been described in detail[11]. In summary, 20 g of MgO was mixed with 300 mL of MeOH, the mixture was then pressurized with 4 bar of CO_2 and left to react under stirring for 24 h at room temperature. When the reaction was completed, unreacted MgO was separated from the synthetic liquid by centrifugation. Al_2O_3 or SiO_2 nanoparticles (10 wt.%) were then added to the synthetic liquid and thoroughly dispersed. After that the liquid was dried at 60°C under constant stirring until a white powder was formed. The obtained powder sample was then dried at 150 °C overnight. The MMC sample without Al or

Si was obtained in the same way but without the addition of Al_2O_3 or SiO_2. The MMC samples containing Al_2O_3 or SiO_2 are referred to as MMC-Al and MMC-Si, respectively.

2.2. Preparation of NiO/ MgO(-Al, -Si)

MMC, MMC-Al and MMC-Si were loaded with 10 wt.% Ni through impregnation. A $Ni(NO_3)_2$ (Tianjin Kemiou Chemical Reagent Co., Ltd., China) aqueous solution was used to impregnate Ni to the MMC samples by the incipient wetness impregnation method carried out for 12 h in room temperature. The samples were thereafter dried at 110 °C for 12 h and then calcined at 500°C for 3 h in air to obtain Ni/MgO catalysts.

2.3. CO methanation

CO methanation reaction was performed in a fixed bed reactor under 0.1 MPa at different temperatures, with a gas flow of 50 mL/min and a ratio H_2/CO of 3. The catalyst (0.2 g) was firstly blended with 0.5 g of silica sand (similar size with catalyst) and then placed in the reactor packed between two parts of quartz wool. The catalyst was then heated up to 550 °C in Ar (50 mL min^{-1}) at a constant heating rate of 10 °C min^{-1}. Afterwards, the catalyst was reduced in H_2 (50 mL min^{-1}) for 2 h. After the reduction, the temperature was declined to 300 °C in Ar and then switched to the feed gas. The catalytic performance was tested at the reaction temperature of 300, 325, and 350 °C. The outlet gas was analyzed online using a gas chromatograph (GC) equipped with a TCD detector and a 2 mTDX-01 packed column, using Ar as the carrier gas. An ice trap was placed between the outlet of the reactor and the GC to remove the moisture.

The conversion of CO, CH_4 selectivity and yield were calculated using the below equations:

CO conversion: $X_{CO}\ (\%)=(F_{CO,in}-F_{CO,out})\times 100/F_{CO,in}$

CH4 selectivity: $S_{CH4}(\%)=F_{CH4,out}\times 100/(F_{CO,in}-F_{CO,out})$

CH4 yield: $Y_{CH4}(\%)=X_{CO}\times S_{CH4}/100=(F_{Ch4,out}\times 100)/F_{CO,in}$

Here, X_{CO} is the conversion of CO, S_{CH4} represents the selectivity of CH_4, Y_{CH4} is the CH_4 yield, and $F_{X,\ in}$ and $F_{X,\ out}$ are the volume flow rates of species X (X = CO or CH_4) at the inlet and outlet, respectively.

2.4 Characterization methods

2.4.1. X-ray diffraction (XRD)

XRD analysis were carried out on a Shimadze XRD-6000 equipment using Cu Kα radiation in the 2θ range of 10°–80°, with the step size and counting time of 0.02° and 10 s, respectively.

2.4.2. Field emission scanning electron microscope (SEM)

SEM images were obtained using a JEOL JSM-6700F.

2.4.3. Transmission elector microscopy (TEM)

TEM analysis and STEM-EDX analyses were carried out on a FEI Tecnai G^2-F20 system operated at 200 kV.

2.4.4. Nitrogen adsorption

Nitrogen adsorption–desorption isotherms were measured at 77 K on a Quantachrome QUADRASORB SI. The samples were degassed at 613 K under vacuum for 3 h before the measurements. The surface area was calculated using the BET equation, and the external surface area and micropore volume were obtained from the t-plot method. Pore size distribution was calculated using a non-local-density functional theory (NLDFT) method with a cylinder pore model included in the Quantachrome software.

2.4.5. X-ray photoelectron spectroscopy (XPS)

XPS was carried out on an ESCALAB250Xi X-ray photoelectron spectrometer with a monochromatic X-ray source manufactured by Thermo. The binding energy was calibrated using the C 1s peak (284.6eV).

3. Results and discussion

3.1. Characterization of the MMC supports and Ni catalysts

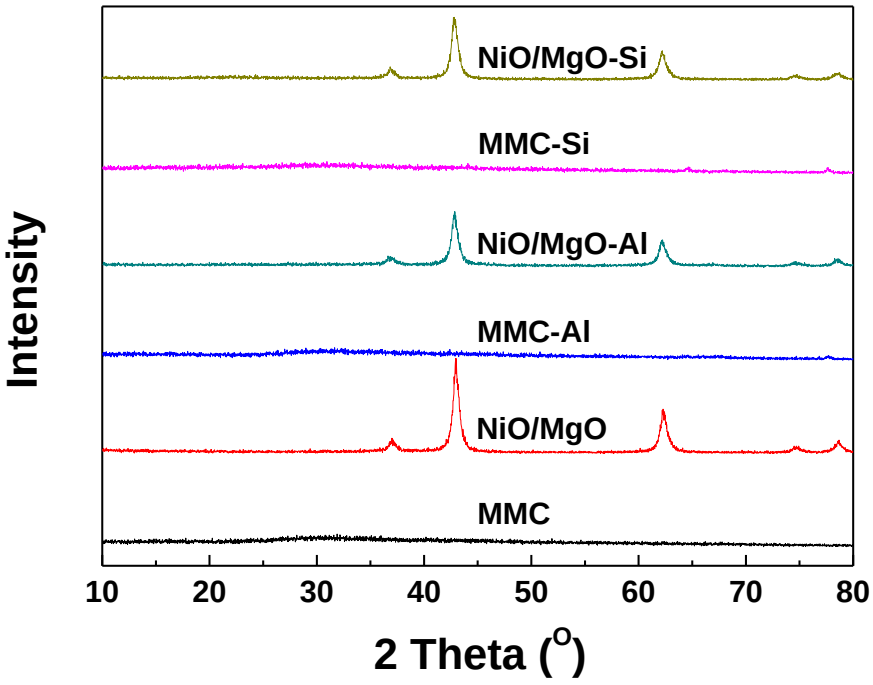

Figure 1. XRD patterns of $MgCO_3$s and NiO/MgOs

The powder XRD patterns of the synthesized MMC supports (MMC, MMC-Si and MMC-Al), shown in Figure 1, demonstrated that all the samples were X-ray amorphous. Ni was supported onto MMC by impregnation method and then calcined at 500 ºC in order to obtain the NiO containing NiO/MgO, NiO/MgO-Si and NiO/MgO-Al catalysts. The powder XRD patterns of these catalysts are also shown in Figure 1. The characteristic peaks of NiO were observed in all three catalysts. The lack of other peaks in the powder XRD patterns meant that the MMC based supports remained amorphous. There was a clear difference in the intensities of the XRD peaks related to NiO. The Scherrer equation was used to estimate the crystal size from XRD data. The crystal sizes of NiO in NiO/MgO, NiO/MgO-Al and NiO/MgO-Si were estimated to be 9.83 nm 8.45 nm and 9.11 nm, respectively. The presence of Al appeared to have resulted in a decreased NiO crystal size. The SEM images of the MMC based supports and the calcined NiO containing catalysts are shown in Figure 2. The general morphology of MMC (Figure 2a), MMC-Si (Figure 2c) and MMC-Al (Figure 2e) resemble that previously shown by Cheung et al [11].The SEM images of calcined NiO/MgO, NiO/MgO-Si and NiO/MgO-Al catalysts showed that the morphology of the MMC support was retained during Ni impregnation and calcination.

In all cases, the MMC based supports as well as the NiO containing catalysts appeared to be irregularly shape particles constructed with an assembly of nanometer-sized particles. As discussed in previous studies, the porosity of MMC arises from the space between these nanometer-sized particles[11].

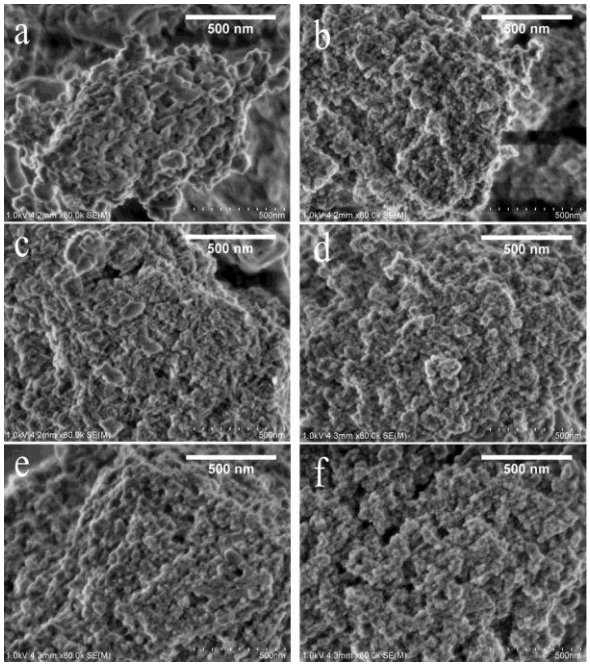

Figure 2. SEM images of a) $MgCO_3$, b) NiO/MgO, c) $MgCO_3$-Al, d) NiO/MgO-Al, e) $MgCO_3$-Si, f) NiO/MgO-Si

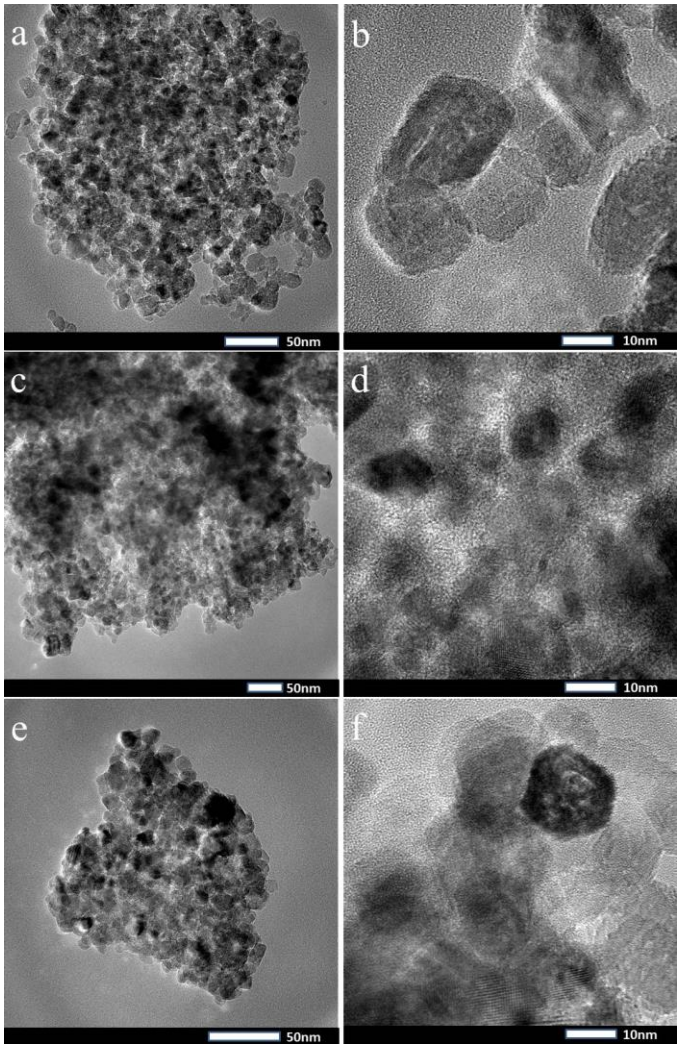

Figure 3. TEM images of a,b) NiO/MgO, c,d) NiO/MgO-Al, e,f) NiO/MgO-Si

The TEM images of NiO/MgO, NiO/MgO-Si and NiO/MgO-Al are shown in Figure 3. The TEM images confirmed that the nanostructure of NiO/MgO, NiO/MgO-Si and NiO/MgO-Al was similar to the previously reported MMC. NiO/MgO, NiO/MgO-Si and NiO/MgO-Al were constructed from nanoparticles that have assembled to form irregularly shaped catalyst particles. The presence of NiO could also be clearly observed. The nanometer-sized NiO particles appeared to be darker than their MMC equivalent. The HRTEM images shown in Figure 3b, d and f revealed that the size of these nanometer-sized NiO particles differed between samples. The largest NiO particles were observed when MMC was used as the catalyst support (Figure 3b, ~ 30-40 nm in diameter). The presence of Si and Al on MMC appeared to have had an effect on the size of NiO particles. The NiO particles on NiO/MgO-Al were the smallest of the tested samples (Figure 3f ~10 nm), with NiO/MgO-Si showing slightly larger NiO particles (Figure 3d ~20 nm). Elemental mapping of the different elements can be viewed in supporting information (S1). The N_2 adsorption/desorption isotherms of the MMC supports and the NiO containing catalysts are shown in supporting information (S4, S5 and S6). The MMC, MMC-

Si and MMC-Al supports all showed very high specific BET surface area of over 580 m^2/g and total pore volume over 0.7 cm^3/g (Table 1). MMC with similar BET surface area was previously reported and the introduction of Si and Al did not reduce the overall porosity of MMC. The BET surface area and total pore volume of the catalyst decreased significantly after Ni impregnation and calcination. This was somewhat expected as MMC is known to undergo a certain level of crystallization or particle intergrowth when exposed to water. However, according to the powder XRD pattern of NiO/MgO, NiO/MgO-Si and NiO/MgO-Al, no XRD peaks were observed other than those related to NiO. Furthermore, SEM and TEM images of NiO/MgO, NiO/MgO-Si and NiO/MgO-Al also showed that the nanostructure of these samples largely resembled MMC. The nanometer-sized particles that created the porous structure of the MMC supports remained visible with no particles/crystals larger than the nanometer-size particles (similar to MMC) were observed. Thus we could conclude that the loss of BET surface area and pore volume was probably due to the intergrowth of the nanometer sized particles, rather than a large scale crystallization. The particle intergrowth was probably the result of the material being exposed to water.

Table 1. Textual properties of the $MgCO_3$(-Al, -Si), MgO(-Al, -Si) and NiO/MgO(-Al, -Si)

Sample	S_{BET}	S_{Mic}	S_{Ext}	V_{Mic}	V_{Tol}
$MgCO_3$	631	0	631	0	0.773
$MgCO_3$-Al	773	0	773	0	0.715
$MgCO_3$-Si	586	0	586	0	0.885
MgO	175	0	175	0	0.468
MgO-Al	168	0	168	0	0.440
MgO-Si	185	0	185	0	0.487
NiO/ MgO	81	0	81	0	0.299
NiO/ MgO-Al	76	10	66	0	0.259
NiO/ MgO-Si	90	0	90	0	0.314

The Mg 2p XPS spectra of NiO/MgO, NiO/MgO-Si and NiO/MgO-Al are shown in Figure 4b. The Ni $2p_{3/2}$ binding energy of NiO/MgO-Al was higher than that of NiO/MgO and NiO/MgO-Si. This suggested that the strongest interaction existed between Ni and the support on NiO/MgO-Al catalyst. The strong binding energy of Ni and the support on NiO/MgO-Al

showed the existence of electronic effect caused by the introduction of Al, which resulted in the enrichment of electrons on Ni.

It was clear that the addition of NiO affected the binding energy of Mg on the support. According to the XPS spectra, the presence of Si and Al affect the binding energy of the Mg-O peak, as the same peak appeared at a higher binding energy in pure MgO (Figure 4b bottom). The addition of NiO further affected the Mg-O bonding as demonstrated by a shift in the Mg-O peak. The magnitude of this shift was the same for NiO/MgO-Si and NiO/MgO-Al when compared with MgO-Si and MgO-Al, but a much large peak shift was observed for NiO/MgO when compared with MgO. These results suggested that NiO-MgO interaction was the strongest in NiO/MgO, and this same interaction was weaker in NiO-MgO-Si and NiO/MgO-Al.

The surface elemental composition according to the XPS analysis is shown in Table 2. As expected, Mg was the most abundant metal atom on the surface of all of the catalysts. Interestingly, the Ni content was the highest on the surface of the NiO/MgO-Al catalyst, the Ni/Mg(+Al/Si) content was 0.054 (compared to 0.035 for Ni/MgO and 0.047 for Ni/MgO-Si). This suggested that Ni was most dispersed when MMC-Al support was used during Ni impregnation.

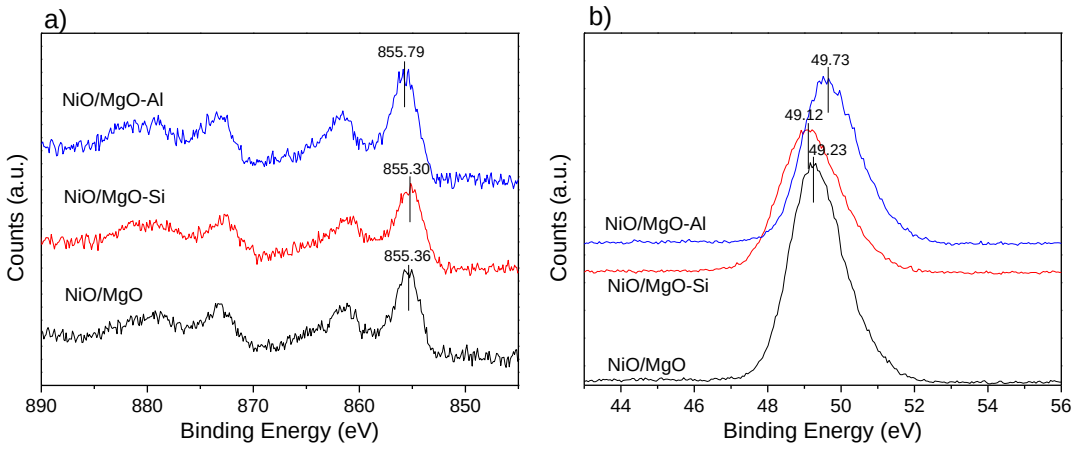

Figure 4. Ni 2p (a) and Mg 2p (b) XPS spectra of the NiO/MgO(-Al, -Si) catalysts

Table 2. XPS data of NiO/MgO(-Al, -Si) catalysts

Catalysts	Elements (At. %)						
	Mg 2p	Al 2p3	Si 2p	Ni 2p	C 1s	O1s	Ni/(Mg(+Al/ Si)
NiO/MgO	40.95	0.76	-	1.45	9.73	47.1	0.035
NiO/MgO-Al	36.42	2.16	-	1.99	13.93	45.50	0.052
NiO/MgO-Si	38.11	0.69	2.73	1.81	8.37	48.29	0.047

3.2. CO methanation

The Ni/MgO, Ni/MgO-Si and Ni/MgO-Al were tested as catalysts in a CO methanation reaction at three different temperatures (300, 325 and 350 °C). All three materials were able to catalyze the CO methanation reaction. According to the corresponding CO conversion and CH_4 yield shown in Figure 5a and b, 350 °C was required to achieve high CO conversion and high CH_4 yield, irrespectively to the catalyst used. At all temperatures tested, NiO/MgO-Al showed the best performance out of all the tested catalysts. The CO conversion reached close to 100% at 350 °C when NiO/MgO-Al was used as the catalyst with a CH_4 yield of around 75 %. NiO/MgO-Si performed reasonably well at 300 and 325 °C with higher CO conversion and CH_4 yield than NiO/MgO, but this trend was reversed when the methanation temperature was increased to 350 °C. At 350 °C, the CO conversion was ~70 % for NiO/MgO and around 64 % for NiO/MgO-Si. The CH_4 yield for NiO/MgO at 350 °C was around 60 % and 55 % for NiO/MgO-Si. The CH_4 selectivity of the different catalysts at different temperatures are presented in Figure 5c. In contrast to the CO conversion and CH_4 yield, the CH_4 selective was the highest at 300 °C for all three catalysts. Furthermore, NiO/MgO had the highest CH_4 selectivity at all three tested temperatures. The CH_4 selectivity of NiO/MgO at 300 and 325 °C was close to 100 %, and dropped to around 83 % at 350 °C. For comparison the CH_4 selectivity of NiO/MgO-Al at 350 °C was around 75 %.

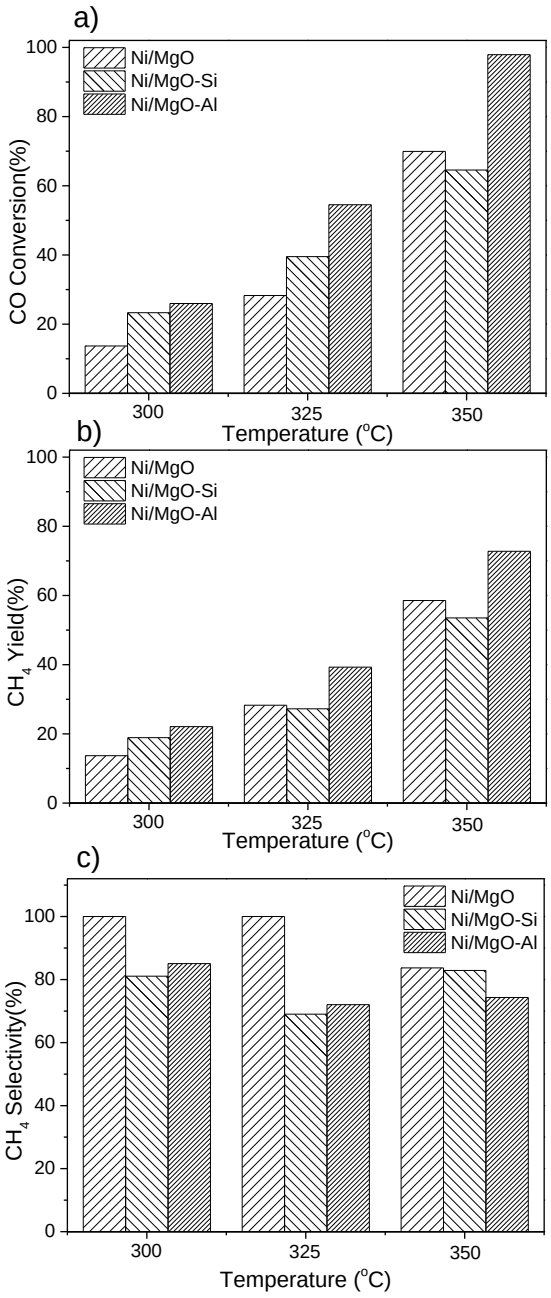

Figure 5. CO conversion, CH4 yield and CH4 Selectivity of Ni/MgO, Ni/Mg-Al and Ni/MgO-Si at low reaction temperatures.

The best performing catalyst – NiO/MgO-Al was further tested at different reaction temperatures. The CO conversion, CH_4 selectivity and CH_4 yield at different temperatures (ranging from 300 to 550 °C) is shown in Figure 6. According to Figure 6, a further increase in temperature above 350 °C did not increase the performance of the NiO/MgO-Al catalyst. At temperatures above 450 °C the performance of the NiO/MgO-Al catalyst was adversely affected.

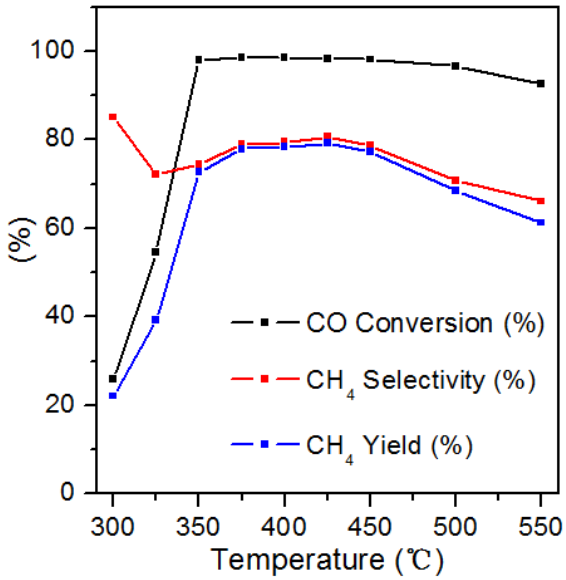

Figure 6. CO conversion, CH4 Selectivity, and CH4 yield of Ni/MgO-Al at different reaction temperatures.

4. Conclusions

Three different supports for Ni catalyst were synthesized (MMC, MMC-Si and MMC-Al). The different supports were then impregnated by $Ni(NO_3)_2$ and calcined at 500 °C creating NiO/MgO, NiO/MgO-Al and NiO/MgO-Si. XRD, XPS and EDS confirmed the presents of NiO in all samples. N_2 sorption showed that the impregnation of Ni had an effect on the porosity of the MMC based supports, but all MMC supports were still porous after impregnation and calcination. The three catalysts were then evaluated on their catalytic performance over a range of temperatures. Results showed that an addition of Al_2O_3 nanoparticles to the NiO/MgO catalyst significantly improved its performance with a CO conversion close to 100 %, and a CH_4 selectivity and yield over 70 % at 350 °C.

References

[1] J. Gao, Q. Liu, F. Gu, B. Liu, Z. Zhong, F. Su, *RSC Adv.* **2015**, 5, 22759.

[2] P. Sabatier, J. B. Senderens, *C. R. Acad. Sci. Paris* **1902**, 134.

[3] J. Kopyscinski, T. J. Schildhauer, S. M. A. Biollaz, *Fuel* **2010**, 89, 1763.

[4] L. Zhang, D.-X. Gu, Y. liu, Y. Zhang, *Catal. Lett.* **2017**, 147, 1172.

[5] X. Yan, C. Yuan, J. Bao, S. Li, D. Qi, Q. Wang, B. Zhao, T. Hu, L. Fan, B. Fan, R. Li, F. Tao, Y.-X. Pan, *Catal Sci Technol* **2018**, 8, 3474.

[6] C. Cheng, D. Shen, R. Xiao, C. Wu, *Fuel* **2017**, 189, 419.

[7] V. Šnajdrová, T. Hlinčík, K. Ciahotný, L. Polák, *Chemical Papers* **2018**, 72, 2339.

[8] D. Hu, J. Gao, Y. Ping, L. Jia, P. Gunawan, Z. Zhong, G. Xu, F. Gu, F. Su, *Ind. Eng. Chem. Res.* **2012**, 51, 4875.

[9] X. Wang, Q. Liu, J. Jiang, G. Jin, H. Li, F. Gu, G. Xu, Z. Zhong, F. Su, *Catal Sci Technol* **2016**, 6, 3529.

[10] J. Forsgren, S. Frykstrand, K. Grandfield, A. Mihranyan, M. Strømme, *PLoS One* **2013**, 8, e68486.

[11] O. Cheung, P. Zhang, S. Frykstrand, H. Zheng, T. Yang, M. Sommariva, X. Zou, M. Stromme, *RSC Adv.* **2016**, 6, 74241.

Supporting Information

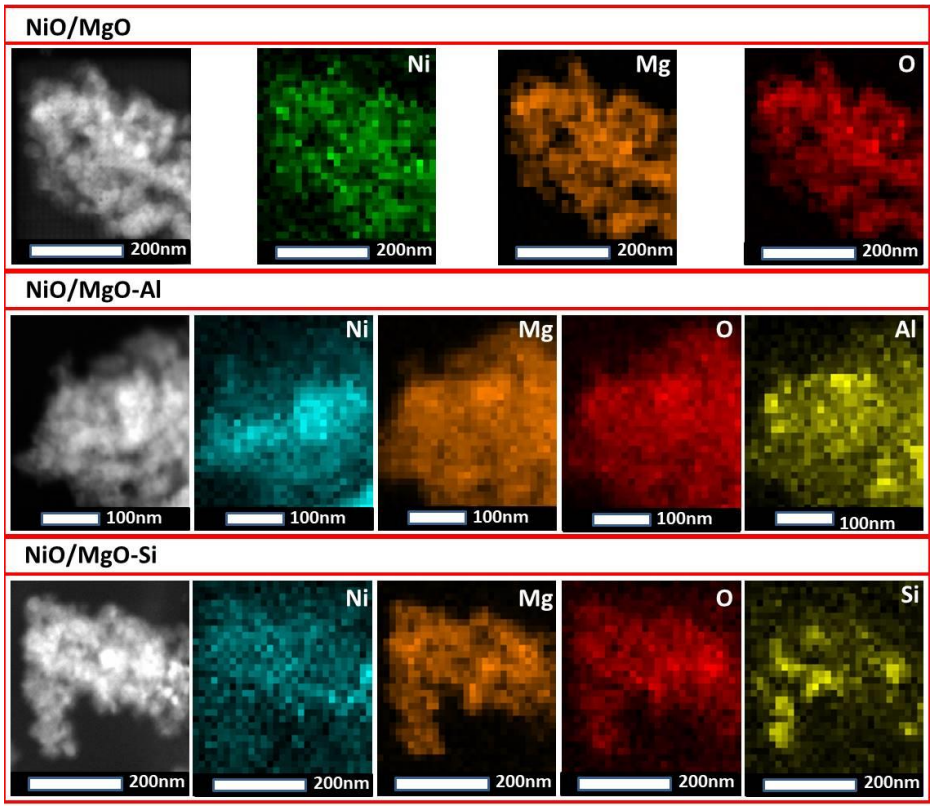

Figure S1. Elemental mapping patterns of NiO/MgO, NiO/MgO-Al and NiO/MgO-Si.

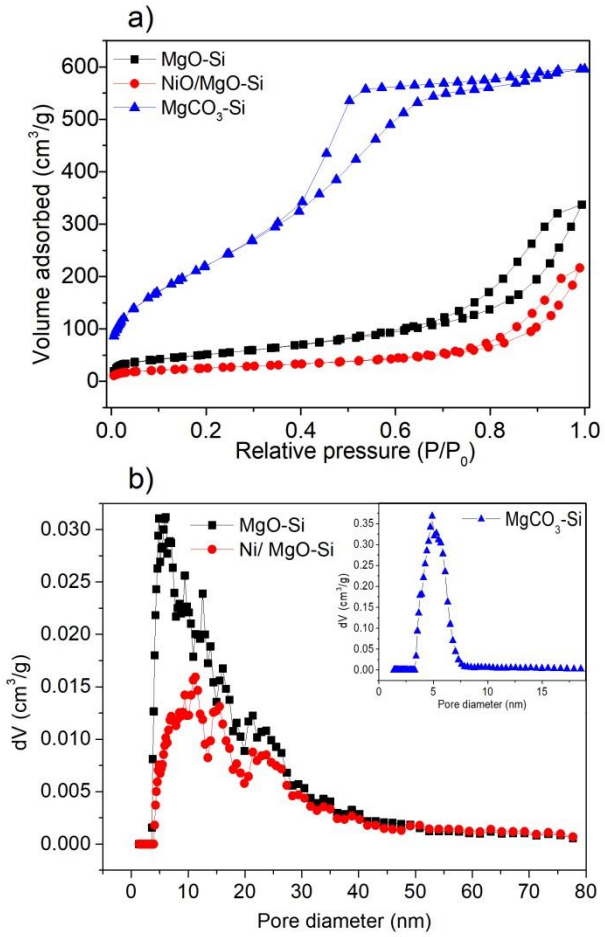

Figure S2. Nitrogen adsorption isotherms of and pore size distribution for MgO-Si, NiO/MgO-Si and $MgCO_3$-Si

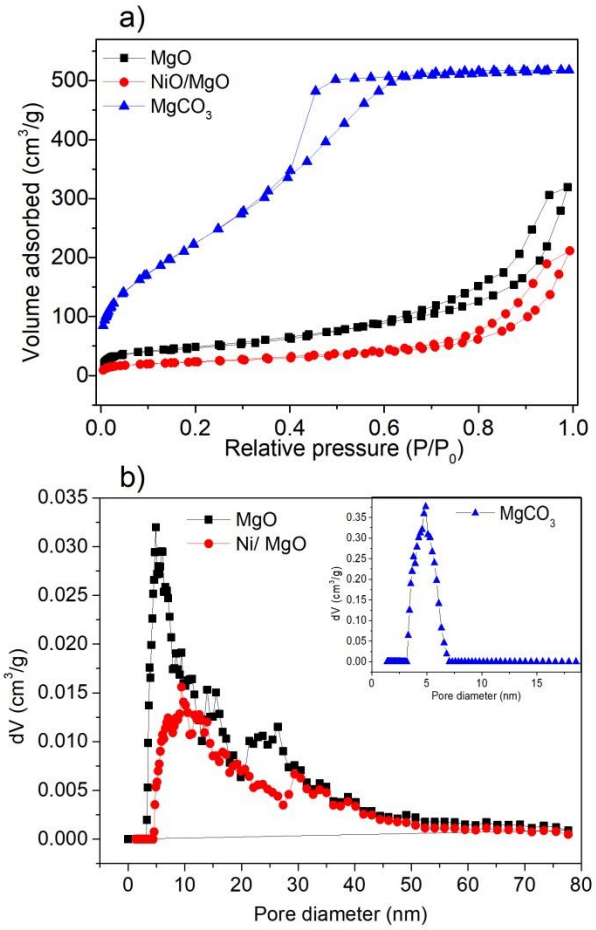

Figure S3. Nitrogen adsorption isotherms of and pore size distribution for MgO, NiO/MgO and $MgCO_3$

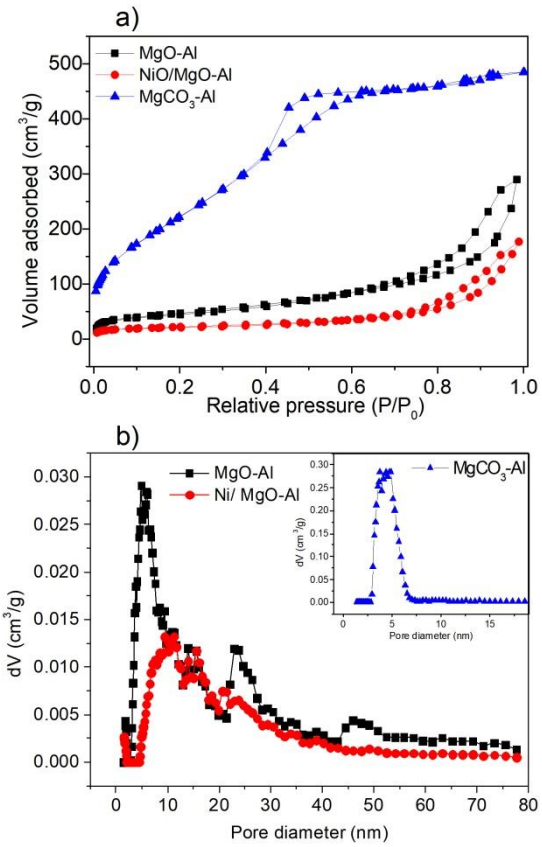

Figure S4. Nitrogen adsorption isotherms of and pore size distribution for MgO-Al, NiO/MgO-Al and $MgCO_3$-Al